Hindawi Publishing Corporation
Advances in Civil Engineering
Volume 2014, Article ID 156926, 8 pages
http://dx.doi.org/10.1155/2014/156926

Research Article

Experimental and Numerical Evaluation of Direct Tension Test for Cylindrical Concrete Specimens

Jung J. Kim[1] and Mahmoud Reda Taha[2]

[1] *School of Architecture, Kyungnam University, Changwon-si 631-701, Republic of Korea*
[2] *Department of Civil Engineering, University of New Mexico, Albuquerque, NM 87131, USA*

Correspondence should be addressed to Mahmoud Reda Taha; mrtaha@unm.edu

Received 14 April 2014; Accepted 22 May 2014; Published 19 June 2014

Academic Editor: Serji N. Amirkhanian

Concrete cracking strength can be defined as the tensile strength of concrete subjected to pure tension stress. However, as it is difficult to apply direct tension load to concrete specimens, concrete cracking is usually quantified by the modulus of rupture for flexural members. In this study, a new direct tension test setup for cylindrical specimens (101.6 mm in diameter and 203.2 mm in height) similar to those used in compression test is developed. Double steel plates are used to obtain uniform stress distributions. Finite element analysis for the proposed test setup is conducted. The uniformity of the stress distribution along the cylindrical specimen is examined and compared with rectangular cross section. Fuzzy image pattern recognition method is used to assess stress uniformity along the specimen. Moreover, the probability of cracking at different locations along the specimen is evaluated using probabilistic finite element analysis. The experimental and numerical results of the cracking location showed that gravity effect on fresh concrete during setting time might affect the distribution of concrete cracking strength along the height of the structural elements.

1. Introduction

Concrete cracking strength is difficult to be quantified and therefore is a source of considerable uncertainty in serviceability prediction. The existence of cracks under service load in reinforced concrete (RC) structures makes it difficult to predict deflections. While cracked concrete is usually assumed to be incapable of carrying tensile stresses, the concrete between adjacent cracks can resist tensile force due to the bond between concrete and steel reinforcement. This is known as tension stiffening effect. Therefore, for the consideration of the deflections of RC structures, concrete cracking strength affects the structural stiffness of the members. Moreover, cracking plays an important role in the durability of RC structures. When concrete cracks, its permeability increases and the processes of concrete deterioration and rebar corrosion get accelerated [1, 2].

For flexural elements, concrete cracking is usually represented by the modulus of rupture [3]. However, in research experiments, the modulus of rupture showed a wide variation [4, 5]. While the modulus of rupture provides a good estimate for cracking strength, researchers showed that accurate serviceability predictions require obtaining the real tensile strength of concrete [6]. Moreover, researchers have argued that, because of the significance of shrinkage on serviceability of RC structures, other cracking criteria, such as the direct or indirect tensile strength of concrete, should be used as evidence of concrete cracking [7]. Three methods are commonly used to measure concrete cracking strength: flexural, splitting, and direct tension test. While the flexural strength test and splitting tensile strength test can be conducted in accordance with the American standard test method (ASTM), ASTM C 78 [8] and ASTM C 496/C 496M [9], respectively, ASTM has no recommendations for direct tension test for concrete, as it is challenging to ensure that uniaxial stress along the specimen is evenly applied.

Several methods have been proposed for direct tension test, such as using friction grip, anchor, and epoxy, to attach

the loading machine and concrete specimen. However, all these methods induce secondary stresses that result in an uneven stress application to concrete specimens [10]. To make the applied point load a more evenly distributed load, US Bureau of Reclamation [11] proposes the use of a double plate system for two sizes of diameters of 152.4 mm and 254 mm cylinder specimens. The outer plate is connected to a loading machine, while the inner plate is bonded with the concrete specimen with epoxy. The inner and outer plates are connected to each other by bolts. Recently, this method was modified for the rectangular section of 100 mm by 100 mm and showed acceptable results [10].

In this study, the above method is further developed for cylindrical specimen (101.6 mm in diameter and 203.2 mm in height). Moreover, the stress uniformity of the proposed direct tension test method is evaluated using the finite element method. The stress uniformity along the specimen is compared with the stress uniformity of the direct tension test for rectangular specimen. As experimental results showed that the cracking location was concentrated at the top half of the vertically cured cylindrical specimens, the unit weight of the two broken parts was measured to examine the effect of unit weight on cracking strength and cracking location.

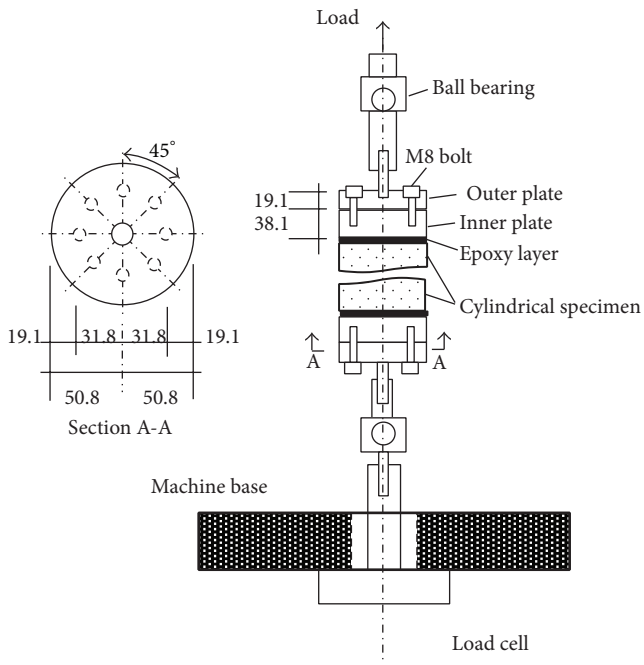

Figure 1: Test setup of the proposed direct tension test for 101.6 mm diameter and 203.2 mm height cylinder (mm).

2. Proposed Test Setup

For the cylinder size of 101.6 mm diameter and 203.2 mm height, a double plate system with epoxy adhesive was adopted for the direct tension test setup as shown in Figure 1. The intention is to use cylinders similar to those used to evaluate the compressive strength of concrete in the concrete industry. The inner and outer plates were connected to each other by eight high-strength bolts. Tension load was applied through ball bearings in order to prevent the developing of bending and torsion stresses in the concrete specimen. The thickness of the inner plate was determined to be 38.1 mm according to the US Army Engineer Research and Development Center (ERDC), CRD-C 164-92 [12]. It was proposed that the thickness of the end plate should be higher than one third of the diameter of the test specimen. The thickness of the outer plate was chosen as one half of that of the inner plate. The bolting locations of the inner and outer plates were optimized by finite element analysis to get uniform stress distribution. The direct tension test conducted using the proposed test setup is shown in Figure 2.

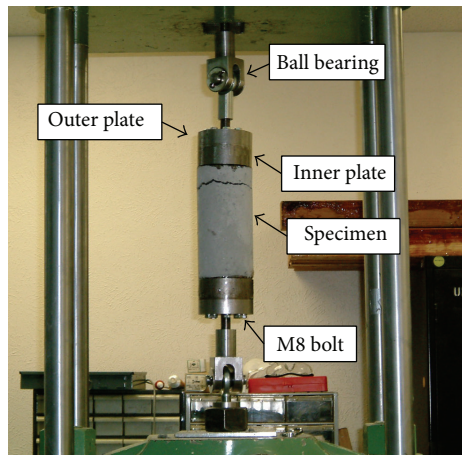

Figure 2: Direct tension test conducted by the proposed test setup.

3. Finite Element Analyses

Linear elastic finite element analyses were performed to investigate the stress distribution along the cylindrical and rectangular specimen, as proposed by others [10]. ANSYS® 7.11 [13] was used for the finite element analyses. The test setups were modeled as 3D solid models. The epoxy, double end plates, and concrete were modeled using SOLID 45 [13], which is a solid cubic element with eight nodes having three degrees of freedom (DOF) for translations about the nodal x, y, and z at each node. The material properties used for finite element analysis are presented in Table 1. The bolt connecting the outer and the inner plates was modeled using LINK 8 [13], three-dimensional (3D) uniaxial tension-compression element with three DOF for translations about the nodal x, y, and z at each node.

The finite element analyses of the test setups for cylindrical and rectangular specimens are conducted. It is important to emphasize that the purpose of numerical modeling is to quantify the uniformity of the stress distribution in the tension specimen and not to examine cracking behavior of the concrete specimen. Therefore, only linear elastic region of concrete constitutive model is used for finite element analyses. Considering the symmetry of the test specimen and loading, a quarter of the specimen's section and a half of the specimen's length were modeled. The boundary conditions

Table 1: Material properties used in finite element analysis.

Materials	Modulus of elasticity (GPa)	Poisson's ratio
Steel	200	0.3
Concrete	22	0.2
Epoxy	1	0.3

of the finite element models were adjusted to simulate symmetry conditions. For the finite element model of the cylindrical specimen, 320 solid elements in 8 layers were used to represent the outer steel plate while 640 solid elements in 8 layers were used to represent the inner steel plate. For the finite element model of the rectangular specimen, 400 solid elements in 4 layers were used to represent the outer steel plate while 800 solid elements in 8 layers were used to represent the inner steel plate. Concrete specimens for the cylindrical and rectangular specimens were modeled with 1600 and 2000 solid elements in 20 layers, respectively. The bolts were modeled using 3 line elements with compressive initial strain of 0.1% to model the bolting force that was initially applied when the outer and inner plates were connected. Using these finite element models, stress distributions were obtained to quantify stress uniformity along the concrete specimens.

The relative tensile stress is defined as the ratio of the tensile stress at any point to the average tensile stress calculated as the applied load divided by cross section area. The relative tensile stress is evaluated both at the top of the specimens and along the specimen. This analysis is performed for both cylindrical and rectangular specimens. The results for the cylindrical specimen showed that the relative tensile stresses across the section vary from 0.98 to 1.02 and the variations of stress distributions at the top of the cylinder were within ±2% of the average tensile stress. For the numerical results of the whole cylinder, the relative tensile stresses varied from 0.96 to 1.03 and the variation of stress distribution over the entire cylinder was within ±4% of the average tensile stress. The numerical results for the rectangular section of 101.6 mm by 101.6 mm showed that the relative tensile stresses across the section vary from 0.94 to 1.01, while those of the whole specimen vary from 0.9 to 1.03. The results for the tensile stress distribution at the top of the rectangular specimen of 100 mm by 100 mm agreed with the results reported by Zheng et al. [10].

3.1. Stress Uniformity along the Specimens. Although the significantly low variations of stress for the cylindrical specimen confirmed the uniformity of stress across and along the tension specimen, a method to quantify stress distribution similarity at different heights along the specimen was developed and is presented here. The degrees of similarity between the tensile stress distributions, as produced by the finite element analysis at various cross sections, and the applied tensile stress distribution were quantified. The degree of similarity was determined using principles of fuzzy image pattern recognition [14]. This method is one of the methods to determine the degree of similarity between two images. The method was applied to two-dimensional (2D) slices. The similarity for two images that have the same size and number of pixels was calculated by comparing pixel values normalized to the interval $[0, 255]$. After the images were converted to three monochromatic basic color images in red (R), green (G), and blue (B), the similarity between two pixels was assigned to a pair of pixels in three monochromatic images according to the difference of pixel values according to Tolt and Kalaykov [15] and Su et al. [16] such as

$$\mu_p = \begin{cases} 1 - \dfrac{\text{abs}\left(m_a - m_b\right)}{\alpha}, & \text{if abs}\left(m_a - m_b\right) \le \alpha \\ 0, & \text{otherwise,} \end{cases} \quad (1)$$

where m_a and m_b are the pixel values for the compared two figures a and b. μ_p is the pixel similarity value that represents the degree of similarity of two pixel values given a threshold α. The advantage of such similarity measure is attributed to its ability to credit a degree of similarity between any two pixels with absolute difference less than α. By taking the arithmetic mean of the similarity values for the monochromatic image pairs in R, G, and B, three scalar similarity values that correspond to R, G, and B were obtained. The similarity of the two images was identified by the arithmetic mean of those three similarity values.

Forty images representing the stress contours of 20 layers for each specimen spread at 5.1 mm were generated by the finite element analysis and were used to calculate the similarity of stress distributions along the cylindrical and rectangular specimens. The similarity between the tensile stress distributions at various cross sections is presented in Figure 3 along the specimen. By taking the arithmetic mean of the similarity values along the specimen, the overall similarity of the stress distribution was calculated as 0.933 and 0.921 for the circular specimen and the rectangular specimen, respectively. Given the similarity curves shown in Figure 3 and the mean similarity values, the stresses produced in the cylindrical specimen were more uniform than those of the rectangular specimen.

4. Experimental Methods

Three concrete mixtures with target compressive strengths of 25, 40, and 55 MPa were considered. Three batches of the concrete mixes were made for each target compressive strength case. Nine 101.6 mm in diameter and 203.2 mm in height cylinders and three 101.6 mm × 101.6 mm × 355.6 mm prisms were prepared from each batch of concrete mixture. Ordinary Portland cement and silica fume were used as cementing materials. The maximum size of the coarse aggregate was 10 mm. The particle distributions of the coarse and fine aggregates are presented in Figure 4. The slump of the concrete mixes was maintained between 50.8 and 69.9 mm. The mixture proportions of the concrete mixes are presented in Table 2. The proposed mix was selected to allow comparison of the experimental results of the new proposed test with those published by Zheng et al. [10].

All 9 cylinders and 3 prisms were demolded after one day of casting and left to cure in water until the day of

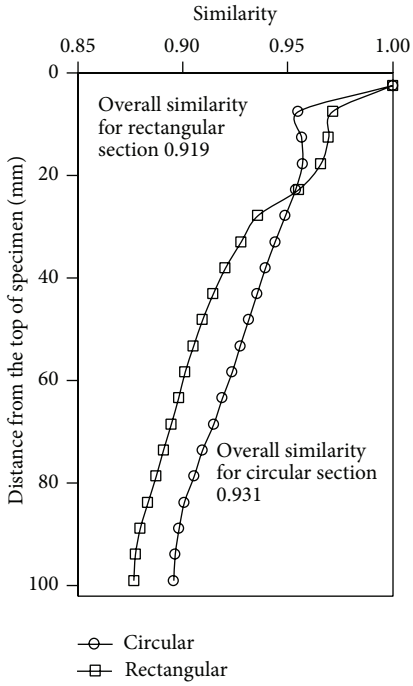

Figure 3: Similarity of stress distribution at each layer to the applied stress distribution for cylindrical and rectangular specimens.

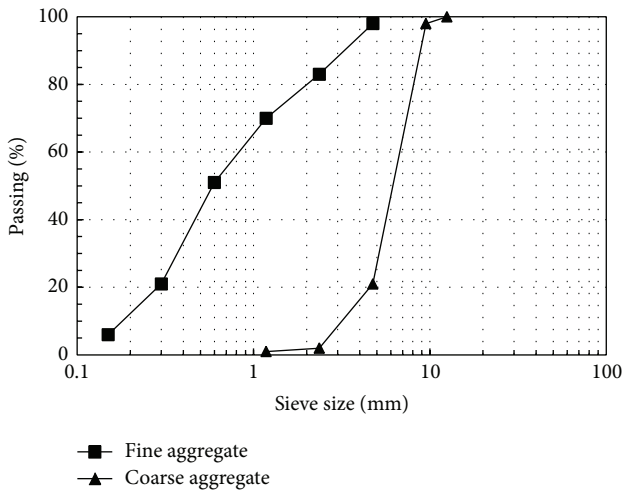

Figure 4: Particle size distributions of the coarse and fine aggregate.

the test. However, 3 cylinders, which were used for direct tension tests, were taken out of the water one day prior to testing. After grinding both sides of each specimen, the specimens were dried for 12 hours and adhered to the steel plates with epoxy, as shown schematically in Figure 1. The epoxy was left for 12 hours to dry to improve bond quality between the concrete specimen and the steel plate in the test setup. The compressive strength test, flexural strength test, and splitting tensile strength test were conducted in accordance with the ASTM C 39/C 39M [17], C 78 [8], and C 496/C 496M [9], respectively. The results are presented in Table 3. The flexural cracking strength of 101.6 mm × 101.6 mm × 355.6 mm prism, splitting cracking strength of cylinder specimens (101.6 mm in diameter and 203.2 mm in height), and direct tensile cracking strength of cylinder specimens (101.6 mm in diameter and 203.2 mm in height) were plotted against the corresponding compressive strength of cylinder specimens (101.6 mm in diameter and 203.2 mm in height) in Figure 5.

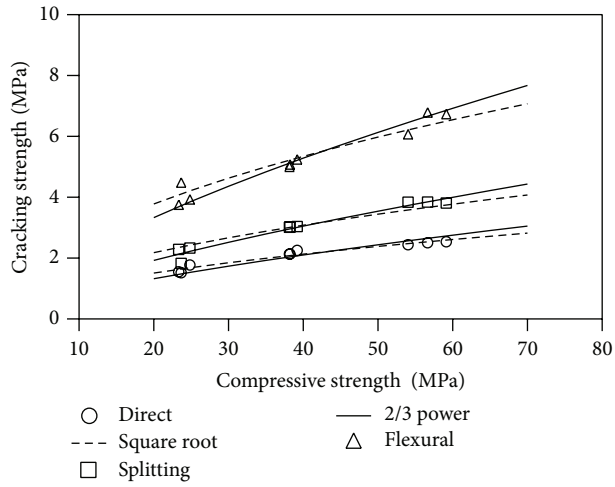

Figure 5: Correlation of various cracking strengths with compressive strength.

For the tests results, the relation between cracking strengths and the corresponding compressive strength was determined in this study based on the assumption that the cracking strength has linear relation with the two third (2/3) power of the corresponding compressive strength as reported by CEB-FIP MC-90 [18]. Regression analysis was performed and the following relations ((2) to (4)) were obtained:

$$f_r = 2.1\left(\frac{f_c'}{10}\right)^{2/3} \text{ (MPa)}, \tag{2}$$

$$f_{sp} = 1.2\left(\frac{f_c'}{10}\right)^{2/3} \text{ (MPa)}, \tag{3}$$

$$f_t = 0.8\left(\frac{f_c'}{10}\right)^{2/3} \text{ (MPa)}, \tag{4}$$

where f_r, f_{sp}, f_t, and f_c' are the flexural tensile strength, splitting tensile strength, direct tensile strength, and compressive strength, respectively. Moreover, test results of cracking strengths were also fitted using regression analysis with the assumption that they have linear relation to the square root of the compressive strength after ACI 318-11 [3]. This analysis results in the following equations:

$$f_r = 0.85\sqrt{f_c'} \text{ (MPa)}, \tag{5}$$

$$f_{sp} = 0.49\sqrt{f_c'} \text{ (MPa)}, \tag{6}$$

$$f_t = 0.34\sqrt{f_c'} \text{ (MPa)}. \tag{7}$$

Table 2: Concrete mix proportions (kg/m^3).

Mixture	Portland cement (Type I)	Silica fume	Water	Fine aggregate	Coarse aggregate	Admixture (L/m^3)
M-1	236	79	192	700	1143	0.47
M-2	289	97	185	587	1192	1.57
M-3	345	115	179	479	1232	3.63

Table 3: Results for direct tension tests presenting mean/standard deviation (MPa).

Mix	Batch	Compressive strength	Flexural tensile strength	Splitting tensile strength	Direct tensile strength
M-1	B-1	23.4/1.26	3.75/0.18	2.28/0.15	1.55/0.06
	B-2	24.8/0.82	3.93/0.25	2.33/0.15	1.77/0.12
	B-3	23.7/0.79	4.48/0.23	1.82/0.28	1.52/0.04
Mean/std.		24.0/1.09	4.05/0.38	2.14/0.30	1.61/0.14
M-2	B-4	38.2/1.44	5.07/0.40	3.02/0.24	2.13/0.15
	B-5	38.2/0.35	5.00/0.21	3.01/0.16	2.13/0.07
	B-6	39.2/0.18	5.24/0.16	3.03/0.29	2.25/0.06
Mean/std.		38.5/0.90	5.10/0.26	3.02/0.21	2.17/0.11
M-3	B-7	54.0/1.43	6.07/0.34	3.84/0.13	2.44/0.11
	B-8	59.2/1.56	6.73/0.33	3.80/0.41	2.53/0.08
	B-9	56.7/3.65	6.78/0.41	3.84/0.20	2.50/0.06
Mean/std.		56.6/3.06	6.53/0.47	3.83/0.24	2.49/0.08

The relationship between cracking strengths in this study will be

$$f_r = 1.75 f_{sp} = 2.50 f_t. \quad (8)$$

It is important to note that the direct tensile strength of concrete in (7) is less than half the value proposed by ACI 318-11 [3]. While ACI 318-11 [3] proposes using the modulus of rupture, the use of tensile strength to express cracking has been recommended by many researchers [6, 19]. The proposed tension test should enable a cracking strength limit by ACI 318-11 [3] lower than current limits obtained from the modulus of rupture experiments. It is also noticeable that the regression results for flexural strength test in (2) and (5) lie between the minimum and the average of the regression results reported by Légeron and Paultre [20]. Moreover, the cracking strength models proposed by CEB-FIP MC-90 [18] and ACI 318-11 [3] lie between the regression results of splitting and the flexural strengths.

5. Cracking Location

Although uniform stress was developed in the concrete specimen subjected to tension by the proposed test setup, the cracking failure location in concrete is difficult to predict due to the inherent variations in concrete microstructures. The numerical analysis of the concrete specimen subject to tension shows that uniform stress was developed along the specimen with the assumption that material distribution is homogeneous and the response is linear elastic. If concrete has been properly placed and no variation in the unit weight of concrete along the specimen takes place, the cracking location in the proposed direct tension test is expected to be uniformly distributed along the specimen (i.e., cracking can take place at any location along the specimen). However, direct tension test results of 27 specimens (results in Table 3) by the proposed test setup showed that the cracking location was frequently concentrated in the top one-third of the specimen as shown in Figure 6. Statistical analysis of cracking location proved to be significantly different from mid height. This observation can be attributed to variation of the unit weight of concrete along the specimen. The increase in unit weight towards the bottom is a well-known phenomenon due to higher consolidation with gravity at the bottom than at the top of the specimen [21].

To confirm this hypothesis, the unit weights of the two broken parts of all specimens tested by the direct tension test were measured. These measured unit weights were plotted according to the distance from the top of the specimen to the center of the measured parts as shown in Figure 7. A linear relationship between the unit weight $w(x)$ and the distance from the top of the specimen x in mm is determined as

$$w(x) = 0.789x + 2352.7 \left(\frac{\text{kg}}{\text{m}^3}\right) \quad (0 \le x \le 203.2\,\text{mm}). \quad (9)$$

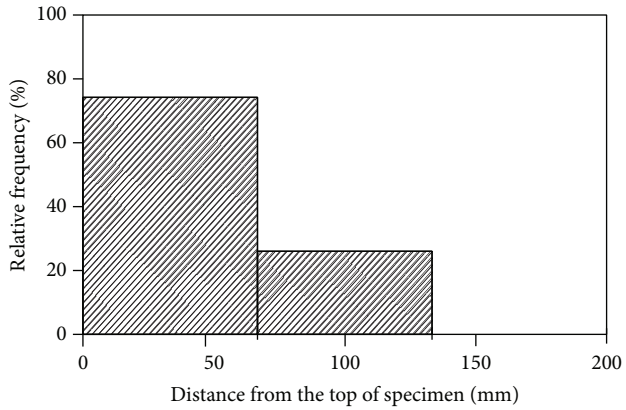

Figure 6: Cracking location measured from the top of specimen.

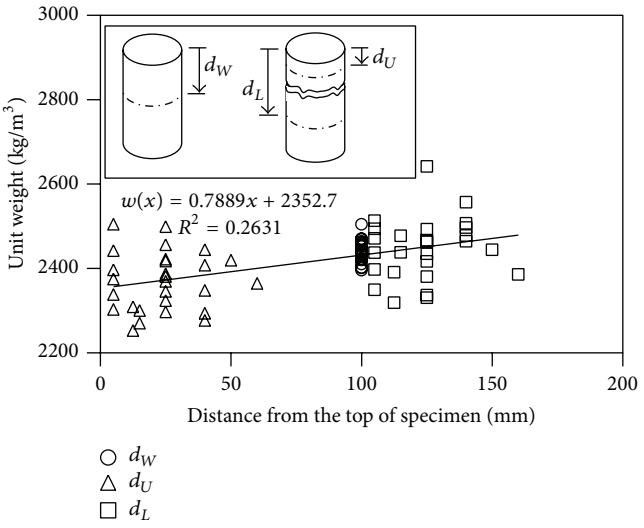

Figure 7: Unit weight distribution along the specimen height.

By considering the modulus of elasticity computational model that incorporates the unit weight [3], the modulus of elasticity variation along the specimen is calculated as

$$E(x) = 0.043 w(x)^{1.5} \sqrt{f_c'} \text{ (MPa)} \quad (0 \le x \le 203.2 \text{ mm}). \tag{10}$$

With the distribution of modulus of elasticity along the specimen, another set of finite element analyses was conducted. Here, the cylinder was modeled in full height, but a quarter of the section was considered for symmetry conditions. The concrete cylinder was divided into 40 layers and the modulus of elasticity of each layer was calculated using (9) and (10). From the stress distribution along the cylindrical specimen, the maximum stress distribution along the specimen was obtained. By assuming that the maximum tensile stress at each layer is normally distributed, the probability of cracking at each layer can be calculated. As the maximum stress distribution at each layer is independent of that at other's layer, the probability of cracking at each layer can be calculated as

$$p_f(i) = \int \int_{f_i \ge f_j, i \ne j} \cdots \int p_1(f_1)\, p_2(f_2) \cdots p_{40}(f_{40})\, df_1 df_2 \cdots df_{40}, \tag{11}$$

where $p_i(i)$ is the probability density function (PDF) of the maximum stress f_i at a layer i. However, computation of the probability of cracking requires defining the tensile strength distribution along the specimen. Two methods were considered here. First, we consider the tensile strength variation along the specimen $f_t(x)$ with respect to specimen unit weight $w(x)$ according to ACI 209R-92 [22] described as

$$f_t(x) = 0.0069 \sqrt{w(x)\, f_c'} \text{ (MPa)} \quad (0 \le x \le 203.2 \text{ mm}). \tag{12}$$

Second, the tensile strength variation can be derived by considering the correlation between cracking strength and modulus of elasticity, which is conventionally accepted to be fully correlated. Therefore, the tensile strength variation along the specimen $f_t(x)$ can be determined by modifying (7) to vary linearly with the modulus of elasticity as

$$f_t(x) = \frac{E(x)}{E(101.6)} 0.34 \sqrt{f_c'} \text{ (MPa)} \quad (0 \le x \le 203.2 \text{ mm}), \tag{13}$$

where $E(101.6)$ is the modulus of elasticity at the center of the specimen chosen to represent the mean modulus of elasticity of the whole specimen. By defining the tensile strength variation using (12) or (13), the probability of cracking integration in (11) can be computed using the Monte Carlo simulation [23] as

$$p_f(i) = \frac{n\left\{f_i / f_t(i) \ge f_j / f_t(j), i \ne j\right\}}{N}, \tag{14}$$

where $f_t(i)$ and $f_t(j)$ are the cracking strength evaluated at the middle of the ith and jth layers using (12) or (13), respectively. The probabilities of cracking along the specimen were calculated using (14) by considering 4×10^6 sampling iterations for each layer with the coefficient of variation (COV) of the maximum stress taken as 10%.

For two models of tensile strength variation using (12) or (13), the probabilities of cracking along the specimen are presented in Figures 8(a) and 8(b), respectively. The experimental observations of the cracking location in direct tension tests as shown in Figure 6 met the probabilistic prediction confirming the hypothesis of the significance of unit weight variation on cracking location. The probabilistic prediction using the linear variation of the tensile strength with respect to the modulus of elasticity (13) was capable of meeting the experimental observations better than that using the variation proposed by ACI 209R-92 model [22] (12). The experimental and probabilistic prediction results of the cracking location seem to be caused by the effect of gravity on fresh concrete during setting time. Therefore, this might

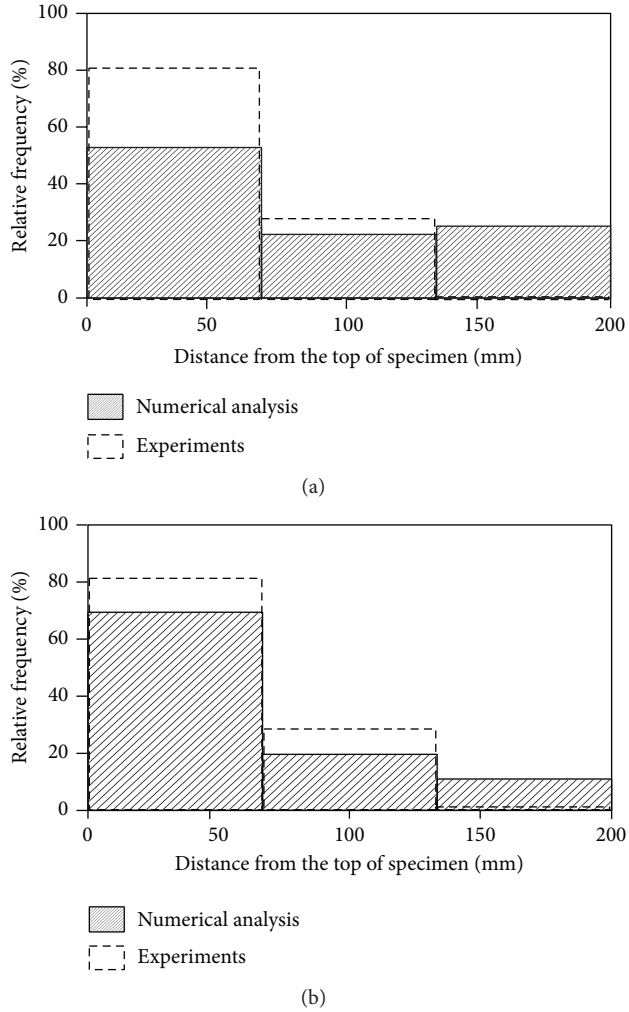

Figure 8: Probability of cracking with the maximum stress COV of 10% when considering the variations of modulus of elasticity and cracking strength along the specimen (a) using (12) and (b) using (13).

be correlated with the properties of fresh concrete. This effect can be exaggerated for relatively deep beams or slabs. In other words, cracking strengths at the top of a structural element would be less than what is predicted by using current design codes. Such variation in concrete properties was observed in bond strength with steel reinforcement [24] and is addressed in development length models by ACI design code [3]. Therefore, when the negative moment is acting on top regions of concrete structural elements, a reduced cracking strength might be considered for conservative serviceability calculations. Further research investigations are needed to confirm the effect of gravity on cracking strength distribution of concrete while considering the significance of aggregate volume fraction, size, and shape.

6. Conclusions

A new test setup of direct tension test for cylindrical concrete specimen (101.6 mm in diameter and 203.2 mm in height) is proposed. Experimental and numerical methods are used to support the proposed test setup. The stress uniformity along the specimen is examined using the finite element method aided by a fuzzy image pattern recognition algorithm. The unit weights distribution along cylindrical concrete specimen (101.6 mm in diameter and 203.2 mm in height) was determined. Measurements confirmed the increase in unit weight towards the bottom of the specimens. Distribution of unit weight is shown to significantly affect the probability of cracking along the tension specimens. The probabilities of cracking along the specimen were also calculated using Monte Carlo simulation. The probabilistic prediction results agree with the experimental observations confirming that cracking location in direct tension tests is a function of unit weight distribution along the specimen.

Notations

a, b: Images that have the same size and number of pixels
$E(x)$: Modulus of elasticity at x in concrete specimen
f'_c: Compressive strength of concrete
f_i, f_j: The maximum stress at ith and jth layer in finite element model
f_r: Flexural strength of concrete (modulus of rupture)
f_{sp}: Splitting tensile strength of concrete
f_t: Direct tensile strength of concrete
$f_t(x)$: Direct tensile strength at x in concrete specimen
i, j: ith and jth layer in finite element model
m_a, m_b: Pixel values for the two figures a and b
$n\{\}$: The number of sampling cases that satisfy the condition in brackets {}
N: Total sampling numbers
$p_f(i)$: Probability of cracking of ith layer
$p_i(f_i)$: Probability density function (PDF) of f_i
$w(x)$: Unit weight at x in concrete specimen
x: Distance from the top of concrete specimen
α: Threshold of similarity
μ_p: Pixel similarity.

Conflict of Interests

The authors declare that there is no conflict of interests regarding the publication of this paper.

Acknowledgments

The first author would like to acknowledge the National Research Foundation (NRF) Grant funded by the Korean government (MOE) (no. 2013R1A1A2062784). The financial support to the second author by the Defense Threat Reduction Agency (DTRA) is also acknowledged.

References

[1] P. K. Mehta and P. J. M. Monteiro, *Concrete, Microstructure, Properties, and Materials*, McGraw Hill, New York, NY, USA, 3rd edition, 2006.

[2] J. G. MacGregor and J. K. Wight, *Reinforced Concrete, Mechanics and Design*, Prentice Hall, Upper Saddle River, NJ, USA, 4th edition, 2005.

[3] ACI Committee 318, *Building Code Requirements for Structural Concrete (318-11) and Commentary (318R-11)*, American Concrete Institute, Farmington Hills, Mich, USA, 2011.

[4] J. M. Raphael, "Tensile strength of concrete," *ACI Journal*, vol. 81, no. 2, pp. 158–165, 1984.

[5] F. A. Oluokun, "Prediction of concrete tensile strength from its compressive strength. Evaluation of existing relations for normal weight concrete," *ACI Materials Journal*, vol. 88, no. 3, pp. 302–309, 1991.

[6] A. Ghali and R. Favre, *Concrete Structures: Stresses and Deformations*, Spon Press, London, UK, 3rd edition, 2002.

[7] M. M. Reda Taha and M. A. Hassanain, "Estimating the error in calculated deflections of HPC slabs: a parametric study using the theory of error propagation," in *Controlling Deflection for the Future*, vol. 210, pp. 65–92, ACI Special Publication, 2003.

[8] ASTM C 78-02, *Standard Test Method for Flexural Strength of Concrete (Using Simple Beam with Third-Point Loading)*, American Standard Test Method, West Conshohocken, Penn, USA, 2002.

[9] ASTM C 496/C 496M-04, *Standard Test Method for Splitting Tensile Strength of Cylindrical Concrete Specimens*, American Standard Test Method, West Conshohocken, Penn, USA, 2004.

[10] W. Zheng, A. K. H. Kwan, and P. K. K. Lee, "Direct tension test of concrete," *ACI Materials Journal*, vol. 98, no. 1, pp. 63–71, 2001.

[11] U.S. Bureau of Reclamation, *Procedure for Direct Tensile Strength, Static Modulus of Elasticity, and Poisson's Ratio of Cylindrical Concrete Specimens in Tension (USBR 4914-92)*, Concrete Manual Part 2, 9th edition, 1992.

[12] CRD-C 164-92, *Standard Test Method for Direct Tensile Strength of Cylindrical Concrete or Mortar Specimens*, U.S. Army Engineering Research and Development Center (ERDC), Vicksburg, Miss, USA, 1992.

[13] SAS, *ANSYS 7.1 Finite Element Analysis SYStem*, SAP IP, 2003.

[14] T. J. Ross, *Fuzzy Logic with Engineering Applications*, John Wiley & Sons, Chichester, UK, 3rd edition, 2010.

[15] G. Tolt and I. Kalaykov, "Measures based on fuzzy similarity for stereo matching of color images," *Soft Computing*, vol. 10, no. 12, pp. 1117–1126, 2006.

[16] M. F. Su, M. M. Reda Taha, C. G. Christodoulou, and I. El-Kady, "Fuzzy learning of talbot effect guides optimal mask design for proximity field nanopatterning lithography," *IEEE Photonics Technology Letters*, vol. 20, no. 10, pp. 761–763, 2008.

[17] ASTM C 39/C 39M-04a, *Standard Test Method for Compressive Strength of Cylindrical Concrete Specimens*, American Standard Test Method, West Conshohocken, Penn, USA, 2004.

[18] CEP-FIP Model Code 90, *Model Code for Concrete Structures, Comité Euro-International du Béton (CEB)—Fédération Internationale de la Précontrainte (FIP)*, Thomas Telford, London, UK, 1993.

[19] R. I. Gilbert, "Shrinkage, cracking and deflection—the serviceability of concrete structures," *Electronic Journal of Structural Engineering*, vol. 1, pp. 15–37, 2001.

[20] F. Légeron and P. Paultre, "Prediction of modulus of rupture of concrete," *ACI Materials Journal*, vol. 97, no. 2, pp. 193–200, 2000.

[21] A. M. Neville, *Properties of Concrete*, Prentice Hall, New York, NY, USA, 4th edition, 1995.

[22] ACI Committee 209, *Prediction of Creep, Shrinkage and Temperature Effects in Concrete Structures (209R-92, Reapproved 2008)*, American Concrete Institute, Farmington Hills, Mich, USA, 2008.

[23] A. H.-S. Ang and W. H. Tang, *Probability Concepts in Engineering: Emphasis on Applications to Civil and Environmental Engineering*, John Wiley & Sons, 2nd edition, 2006.

[24] P. R. Jeanty, D. Mitchell, and M. S. Mirza, "Investigation of top bar effects in beams," *ACI Structural Journal*, vol. 85, no. 3, pp. 251–257, 1988.